GEOPHYSICS, VOL. 41, NO. 4 (AUGUST 1976), P. 766–770, 1 FIG.

SHORT NOTE

DIAGRAMS FOR MAGNETOTELLURIC DATA

F. E. M. LILLEY*

INTRODUCTION

Observed magnetotelluric data are often transformed to the frequency domain and expressed as the relationship

$$\begin{bmatrix} E_1 \\ E_2 \end{bmatrix} = \begin{bmatrix} z_{11} & z_{12} \\ z_{21} & z_{22} \end{bmatrix} \begin{bmatrix} H_1 \\ H_2 \end{bmatrix}, \qquad (1)$$

where E_1, E_2 and H_1, H_2 represent electric and magnetic components measured along two orthogonal axes (in this paper, for simplicity, to be north and east, respectively). The elements z_{ij} comprise the magnetotelluric impedance tensor, and they are generally complex due to phase differences between the electric and magnetic fields. All quantities in equation (1) are frequency dependent. For the special case of "two-dimensional" geology (where structure can be described as having a certain strike direction along which it does not vary), $z_{11} = -z_{22}$ with $z_{12} \neq -z_{21}$. For the special case of "one-dimensional" geology (where structure varies with depth only, as if horizontally layered), $z_{11} = z_{22} = 0$ and $z_{12} = -z_{21}$.

Magnetotelluric tensor characteristics thus reflect geologic structure, and for this to become fully apparent a tensor is often "rotated"; that is, the values of its elements are computed for different hypothetical orientations of the measuring axes (see, e.g., Vozoff, 1972). On a map of several observing sites, the directions of maximum apparent resistivity may then be shown (Dowling, 1970; Reddy and Rankin, 1971), corresponding to the direction in which the E_1-field measurements would be made to obtain a maximum in the absolute value of the element z_{12}. Sometimes polar diagrams are given of the magnitude of one particular tensor element plotted at the angle of rotation of the axes (Berdichevskiy, 1968; Tammemagi and Lilley, 1973). Such polar diagrams for tensor element magnitude are usually not of simple geometric form, as neither would be similar polar diagrams for apparent resistivity.

This note describes some simple figures, mainly conic sections, which display certain characteristics of a magnetotelluric impedance tensor. These figures, which may be plotted on a map, may be useful in showing structural trends and classifying geologic structure as one-, two-, or three-dimensional. For simplicity, the diagrams to be described are based on the real parts of tensor elements and relate the in-phase part of an electric field to its associated magnetic field. In all cases diagrams based on the imaginary parts of tensor elements could be drawn similarly for the quadrature part of an electric field. Also, in cases 1 and 2, diagrams based on the complex values of tensor elements could be drawn for the absolute magnitude of an electric field.

The examples which follow are for an actual field result,

$$\mathbf{z} = \begin{bmatrix} 0.18 & -0.23 \\ 0.16 & -0.12 \end{bmatrix},$$

the real part of the tensor at frequency 0.5 c/hr for station BIL in central South Australia, described by Tammemagi and Lilley (1973).

In this paper, bearings are angles measured clockwise from north. Angle θ is the bearing of a linearly polarized H-field of unit amplitude. Asso-

Manuscript received by the Editor April 28, 1975; revised manuscript received October 23, 1975.
* Australian National University, Canberra A.C.T. 2600, Australia.

ciated with such an H-field is an E-field, the in-phase part of which also is linearly polarized, at bearing ϕ. There may also be a quadrature E-field oscillating with some other linear polarization, so that the total E-field E_c is not linearly polarized: such a quadrature E-field depends upon only the imaginary parts of the tensor elements. Notations E and H denote amplitudes of in-phase E- and H-fields, respectively. Notation z_{ij} refers to the real part of tensor element z_{ij} (except in the third paragraph describing diagram 1).

DIAGRAM 1

It follows from equation (1) that a polar plot of r against θ, where $r = H/E$, has the form

$$r^2[(z_{11}^2 + z_{21}^2)\cos^2\theta + (z_{12}^2 + z_{22}^2)\sin^2\theta + (z_{11}z_{12} + z_{21}z_{22})\sin 2\theta] = 1,$$

which is always an ellipse, and is given for the BIL data in Figure 1a. The lengths of the axes, together with their bearings, can be determined analytically, so that the figure can be drawn without tensor rotation.

The length of a radius of the ellipse gives an inverse measure of the E signal caused by an H oscillation of unit amplitude at the bearing of the radius, and the major and minor axes of the ellipse show the directions of H-field oscillation which give minimum and maximum E-field response, respectively. For two-dimensional geology the ellipse axes will be parallel and perpendicular to geologic strike (see Appendix). For one-dimensional geology the ellipse will widen into a circle of radius $r = |z_{12}|^{-1}$.

If not just the in-phase part of the E-field is considered, but rather the complete E-field (E_c) comprising both in-phase and quadrature parts, then the ellipse generated by plotting $r = H/|E_c|$ at angle θ is of the form

$$r^2[(|z_{11}|^2 + |z_{21}|^2)\cos^2\theta + (|z_{12}|^2 + |z_{22}|^2)\sin^2\theta + (z_{11r}z_{12r} + z_{11i}z_{12i} + z_{21r}z_{22r} + z_{21i}z_{22i})\sin 2\theta] = 1,$$

where the real and imaginary parts of z_{11} are denoted by z_{11r} and z_{11i} respectively, and similarly for z_{12}, z_{21} and z_{22}.

DIAGRAM 2

Similarly, if a plot of r against ϕ is made, taking now $r = E/H$, a figure will be generated of form

$$\frac{r^2}{(z_{11}z_{22} - z_{12}z_{21})^2}[(z_{21}^2 + z_{22}^2)\cos^2\phi + (z_{11}^2 + z_{12}^2)\sin^2\phi - (z_{12}z_{22} + z_{11}z_{21})\sin 2\phi] = 1.$$

This figure is again generally an ellipse, and is shown for the BIL data in Figure 1b.

The length of a radius of the ellipse now gives a measure of the E signal occurring at the bearing of the radius ϕ, when a unit H oscillation occurs at some other bearing θ. The major and minor axes of the ellipse show the directions of the maximum and minimum E oscillations caused by an H oscillation of unit amplitude taking all possible bearings. As for diagram 1, for two-dimensional geology the axes will be parallel and perpendicular to the geologic strike. For one-dimensional geology the ellipse will widen into a circle of radius $r = |z_{12}|$.

DIAGRAM 3

Denoting the component of E perpendicular to H by $E_{\perp H}$, a polar plot of r against θ for $r^2 = H/E_{\perp H}$ will give a figure of form

$$r^2[z_{21}\cos^2\theta - z_{12}\sin^2\theta + (z_{22} - z_{11})\cos\theta\sin\theta] = 1,$$

where the bearing of $E_{\perp H}$ is $(\theta + \pi/2)$. This figure is an ellipse for

$$(z_{22} - z_{11})^2 + 4z_{12}z_{21} < 0,$$

and real or imaginary depending on whether the quantity

$$[(z_{22} - z_{11})^2 + 4z_{12}z_{21}]/(z_{21} - z_{12})$$

is less or greater than zero. For the BIL data, the ellipse is real, and is shown in Figure 1c. The minor and major ellipse axes show which directions of H give the maximum and minimum responses in $E_{\perp H}$, respectively. Generally, the length of the ellipse radius at the H-field bearing of θ gives a measure (in fact the inverse square root) of the associated $E_{\perp H}$ field. For two-dimensional geology, the ellipse axes will be aligned parallel and perpendicular to the geologic strike. For one-dimensional geology, the figure will widen into a circle of radius $r = |z_{21}|^{-1/2}$.

In the case of two-dimensional geology, the ellipse has a further fascinating property. Remembering that $z_{22} = -z_{11}$, the bearing of the tangent

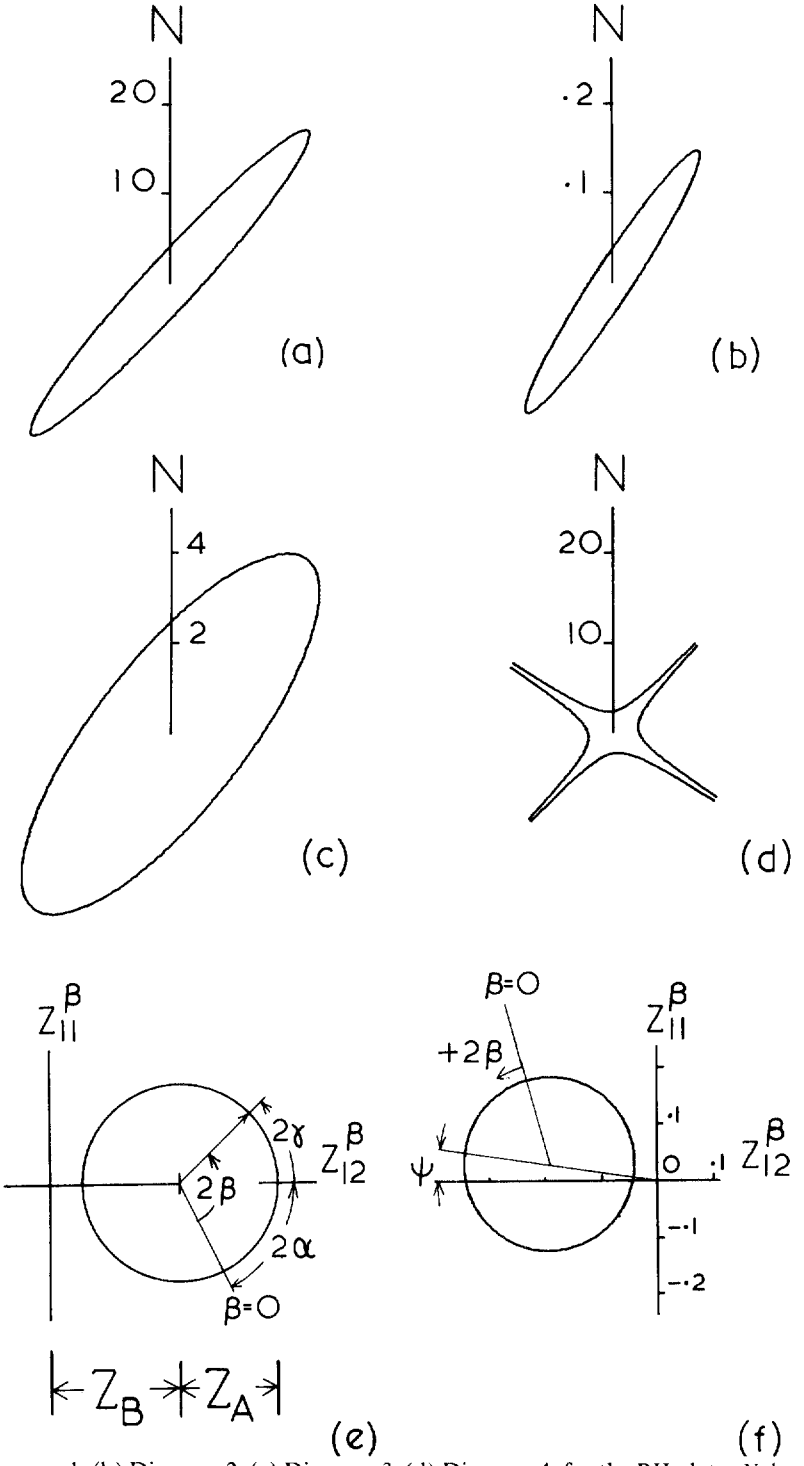

FIG. 1. (a) Diagram 1. (b) Diagram 2. (c) Diagram 3. (d) Diagram 4, for the BIL data. *N* denotes north. (e) A "Mohr circle" for a magnetotelluric impedance tensor measured near two-dimensional geologic structure. (f) A similar Mohr diagram for the BIL data: tan ψ is the "skew".

to the ellipse at the point r, θ is given by

$$\arctan\,[(z_{21} + z_{22}\tan\theta)/(z_{11} + z_{12}\tan\theta)].$$

This angle is also the bearing of the E-field ϕ. Hence, at any point on the ellipse, the tangent gives the direction of E-oscillation associated with an H-oscillation in the radial direction.

DIAGRAM 4

Denoting the component of E parallel to H by $E_{\|H}$, a polar plot of r against θ for $r^2 = H/E_{\|H}$ will give a figure of form

$$r^2[z_{11}\cos^2\theta + z_{22}\sin^2\theta + (z_{12} + z_{21})\cos\theta\sin\theta] = 1.$$

This figure is either an ellipse or a pair of conjugate hyperbolas, depending upon whether the quantity

$$4z_{11}z_{22} - (z_{12} + z_{21})^2$$

is greater or less than zero. On physical grounds only the latter case appears possible, as the former case requires a nonzero $E_{\|H}$ to occur for all possible directions of H-oscillation. The appropriate figures for the BIL data (indeed hyperbolas) are shown in Figure 1d. The asymptotes show the directions of H-oscillation which give only E fields perpendicular to H, and generally the length of a radius at the H-field bearing of θ gives a measure (in fact the inverse square root) of the magnitude of the associated $E_{\|H}$ field.

For two-dimensional geology, the asymptotes become rectangular and perpendicular and parallel to the geologic strike. For one-dimensional geology the figure does not exist, as $E_{\|H}$ does not occur for any H.

DIAGRAM 5

Diagram 5 is not suitable for plotting on a map, but may be useful to display two-dimensionality in magnetotelluric data. The "rotation" of certain tensor elements will be involved, and the various quantities in equation (1) will be marked by a superscript β when referred to axes which have been rotated angle β clockwise from the initial orientation of north and east.

For two-dimensional geology of strike bearing α, equation (1) under rotation becomes (Sims and Bostick, 1969),

$$\begin{bmatrix} E_1^{\beta} \\ E_2^{\beta} \end{bmatrix} = \begin{bmatrix} Z_A\sin 2\gamma & Z_A\cos 2\gamma + Z_B \\ Z_A\cos 2\gamma - Z_B & -Z_A\sin 2\gamma \end{bmatrix} \cdot \begin{bmatrix} H_1^{\beta} \\ H_2^{\beta} \end{bmatrix},$$

where

$$\gamma = \beta - \alpha$$

and

$$Z_A = (z_{12}^{\alpha} + z_{21}^{\alpha})/2,\quad Z_B = (z_{12}^{\alpha} - z_{21}^{\alpha})/2.$$

Thus a plot of z_{11}^{β} against z_{12}^{β} as β varies, where

$$z_{11}^{\beta} = z_{11}\cos^2\beta + (z_{12} + z_{21})\cdot\cos\beta\sin\beta + z_{22}\sin^2\beta,$$

and

$$z_{12}^{\beta} = z_{12}\cos^2\beta + (z_{22} - z_{11})\cdot\cos\beta\sin\beta - z_{21}\sin^2\beta,$$

should produce a circle as shown in Figure 1e. This figure is analogous to the Mohr circle for mechanical stress (see, e.g., Nye, 1957, p. 43).

For the more general case of three-dimensional geology, equation (1) may be written

$$\begin{bmatrix} E_1^{\beta} \\ E_2^{\beta} \end{bmatrix} = \begin{bmatrix} Z_1 - Z_0(\beta + \pi/4) & Z_4 + Z_0(\beta) \\ -Z_4 + Z_0(\beta) & Z_1 + Z_0(\beta + \pi/4) \end{bmatrix} \cdot \begin{bmatrix} H_1^{\beta} \\ H_2^{\beta} \end{bmatrix},$$

where

$$Z_1 = \tfrac{1}{2}(z_{11} + z_{22}),\quad Z_2 = \tfrac{1}{2}(z_{11} - z_{22}),$$
$$Z_3 = \tfrac{1}{2}(z_{12} + z_{21}),\quad Z_4 = \tfrac{1}{2}(z_{12} - z_{21}),$$

and

$$Z_0(\beta) = Z_3\cos 2\beta - Z_2\sin 2\beta.$$

Thus a plot of z_{11}^{β} against z_{12}^{β} as β varies will still produce a circle, with radius $(Z_2^2 + Z_3^2)^{1/2}$, centered at $z_{11}^{\beta} = Z_1$ and $z_{12}^{\beta} = Z_4$.

Such a plot for the BIL data is shown in Figure 1f. The displacement of the center of the circle from the z_{12}^{β} axis gives a measure of the departure of the geology from two-dimensionality; in fact the tan of the angle ψ is the "skew" of the real part of the BIL tensor. From the diagram various values of β of interest can be measured, such as the

one which maximizes z_{12}^{β}, and the two for which z_{11}^{β} is zero.

For one-dimensionality the circle reduces to a point at Z_4 on the z_{12}^{β} axis, as Z_1, Z_2, and Z_3 are all zero.

COMMENTS

Symmetric second-rank tensors occur widely in physics, and diagrams of types 3 and 5 have been used for symmetric cases in various different contexts, as summarized in Nye's book. For two-dimensional geology, diagram 3 in the magnetotelluric case is similar to Nye's (1957, p. 26) "representation quadric", with the difference that the physical property (E) being related to the radial direction is now in the tangential direction of the ellipse rather than in the normal direction. The Mohr circle, diagram 5, commonly has been used for symmetric cases; however, its existence in nonsymmetric cases (Figure 1f) may not be widely known.

Diagrams of types 1 and 2 are not mentioned in Nye's book, but have been introduced by the present author (Lilley, 1974) to depict the "geomagnetic induction tensor", which arises in the analysis of vertical and horizontal magnetic fluctuations.

REFERENCES

Berdichevskiy, M.N., 1968, Electric prospecting by the method of magnetotelluric profiling: Moscow, Nedra.

Dowling, F.L., 1970, Magnetotelluric measurements across the Wisconsin Arch: J. Geophys. Res., v. 75, p. 2683–2698.

Lilley, F.E.M., 1974, Analysis of the geomagnetic induction tensor: Phys. Earth Planet. Inter., v. 8, p. 301–316.

Nye, J.F., 1957, Physical properties of crystals: London, Oxford Press.

Reddy, I.K., and Rankin, D., 1971, Magnetotelluric measurements in central Alberta: Geophysics, v. 36, p. 739–753.

Sims, W.E., and Bostick, F.X., 1969, Methods of magnetotelluric analysis: Univ. of Texas, Austin, Tech. rep. no. 58.

Tammemagi, H.Y., and Lilley, F.E.M., 1973, A magnetotelluric traverse in Southern Australia: Geophys. J.R. Astr. Soc., v. 31, p. 433–445.

Vozoff, K., 1972, The magnetotelluric method in the exploration of sedimentary basins: Geophysics, v. 37, p. 98–141.

ACKNOWLEDGMENTS

Dr. H.Y. Tammemagi is thanked for stimulating discussions on the magnetotelluric impedance tensor several years ago. Dr. D. Rankin and Dr. I.K. Reddy are thanked for providing some numerical data with which the author experimented when visiting the University of Alberta in 1974. Mrs. M.N. Sloane assisted in the computation and preparation of the figures.

APPENDIX

The foregoing note summarizes the results of much algebra, most of which has not been given. As an example of the style of what has been omitted, a proof follows for one of the statements of the paper, regarding diagram 1: "for two-dimensional geology the ellipse axes will be parallel and perpendicular to geologic strike".

For two-dimensional geology, the magnetotelluric impedance tensor has the form given in the first equation under the heading of diagram 5, notably (taking $\beta = 0$)

$$\mathbf{z} = \begin{bmatrix} -Z_A \sin 2\alpha & Z_A \cos 2\alpha + Z_B \\ Z_A \cos 2\alpha - Z_B & Z_A \sin 2\alpha \end{bmatrix}.$$

Substituting these values for z_{11}, z_{12}, z_{21}, and z_{22} into the first equation under the heading of diagram 1, one obtains

$$r^2 = 1/[Z_A^2 + Z_B^2 - 2Z_A Z_B \cos 2(\alpha - \theta)].$$

Now, using the expressions for Z_A and Z_B given in the note, it can be shown that $Z_A^2 + Z_B^2 > |2Z_A Z_B|$; thus, r has minimum and maximum values (defining the axes of the ellipse) when

$$\cos 2(\alpha - \theta) = \pm 1,$$

that is, when θ (the bearing of r) is parallel or perpendicular to α (the geologic strike direction).